International Journal of Heat and Fluid Flow 30 (2009) 679–690

Contents lists available at ScienceDirect

International Journal of Heat and Fluid Flow

journal homepage: www.elsevier.com/locate/ijhff

Effects of variable viscosity and thermal conductivity of Al_2O_3–water nanofluid on heat transfer enhancement in natural convection

Eiyad Abu-Nada *

Department of Mechanical Engineering, Hashemite University, Zarqa 13115, Jordan

ARTICLE INFO

Article history:
Received 18 November 2008
Received in revised form 9 February 2009
Accepted 10 February 2009
Available online 28 March 2009

Keywords:
Nanofluid
Viscosity
Thermal conductivity
Natural convection
Annulus

ABSTRACT

Heat transfer enhancement in horizontal annuli using variable properties of Al_2O_3–water nanofluid is investigated. Different viscosity and thermal conductivity models are used to evaluate heat transfer enhancement in the annulus. The base case uses the Chon et al. expression for conductivity and the Nguyen et al. experimental data for viscosity which take into account the dependence of these properties on temperature and nanoparticle volume fraction. It was observed that for $Ra \geqslant 10^4$, the average Nusselt number was reduced by increasing the volume fraction of nanoparticles. However, for $Ra = 10^3$, the average Nusselt number increased by increasing the volume fraction of nanoparticles. For $Ra \geqslant 10^4$, the Nusselt number was deteriorated every where around the cylinder surface especially at high expansion ratio. However, this reduction is only restricted to certain regions around the cylinder surface at $Ra = 10^3$. For $Ra \geqslant 10^4$, the difference in Nusselt number between the Maxwell Garnett and Chon et al. model prediction is small. But, there was a deviation in prediction at $Ra = 10^3$ and this deviation becomes more significant at high volume fraction of nanoparticles. The Nguyen et al. data and Brinkman model gives completely different predictions for $Ra \geqslant 10^4$ where the difference in prediction of Nusselt number reached 30%. However, this difference was less than 10% at $Ra = 10^3$.

1. Introduction

Natural convection heat transfer is an important phenomenon in engineering systems due to its wide applications in electronic cooling, heat exchangers, and thermal systems. Enhancement of heat transfer in such systems is very essential from the industrial and energy saving perspectives. The low thermal conductivity of conventional heat transfer fluids, such as water, is considered a primary limitation in enhancing the performance and the compactness of such thermal systems. An innovative technique for improvement of heat transfer using nano-scale particle dispersed in a base fluid, known as nanofluid (Choi, 1995), has been studied extensively in recent years (Daungthongsuk and Wongwises, 2007; Trisaksri and Wongwises, 2007) mainly for forced convection applications. However, natural convection heat transfer research using nanofluids has received very little attention and there is still a debate on the effect of nanoparticles on heat transfer enhancement in natural convection applications.

Examples of these controversial results are the results reported by Khanafer et al. (2003) who studied Cu–water nanofluids in a two dimensional rectangular enclosure. They reported an increase in heat transfer with the increase in percentage of the suspended nanoparticles at any given Grashof number. Oztop and Abu-Nada (2008) showed similar results, where an enhancement in heat transfers was registered by the additions of nanoparticles. However, contrary experimental findings were reported by Putra et al. (2003) using Al_2O_3 and CuO water nanofluids. They reported that the natural convection heat transfer coefficient was lower than that of clear flow. Additionally, another experimental work, in natural convection, by Wen and Ding (2006) reported deterioration in heat transfer by the addition of nanoparticles. Most recently, Abu-Nada et al. (2008) showed that the enhancement of heat transfer in natural convection depends mainly on Rayleigh number and for certain Rayleigh numbers, $Ra = 10^4$, the heat transfer was not sensitive to nanoparticles concentration whereas at higher values of Rayleigh number an enhancement in heat transfer was taking place. Therefore, there is still a controversy on the effect of nanofluids on heat transfer in natural convection and the numerical simulations seem to over estimate the enhancement of heat transfer in natural convection.

In fact, convective heat transfer is affected by the thermophysical properties of the nanofluid such as viscosity and thermal conductivity. A recent nanofluid heat transfer study on forced convection conducted by Ben Mansour et al. (2007) revealed that for forced convection different expressions for the thermophysical properties of nanofluids lead to totally different predictions for the performance of system. All of the previous mentioned numerical

* Tel.: +962 390 3333; fax: +962 382 6613.
E-mail address: eiyad@hu.edu.jo

0142-727X/$ - see front matter © 2009 Elsevier Inc. All rights reserved.
doi:10.1016/j.ijheatfluidflow.2009.02.003

Nomenclature

c_p	specific heat at constant pressure (J/kg K)
D	diameter of inner cylinder (m)
g	gravitational acceleration (m/s^2)
h	local heat transfer coefficient (W/m^2 K)
k	thermal conductivity (W/m K)
L	gap between inner and outer cylinder, i.e., $L = r_o - r_i$ (m)
Nu	Nusselt number
Pr	Prandtl number
q_w	heat transfer at the inner cylinder surface (W/m^2)
Ra	Rayleigh number
Re	Reynolds number
$\tilde{r}$	radial coordinate measured from the inner cylinder surface (m)
r	nondimensional radial distance
$\tilde{T}$	dimensional temperature (K)
T	nondimensional temperature
u	dimensional tangential velocity (m/s)
U	nondimensional tangential velocity
v	dimensional radial velocity (m/s)
V	nondimensional radial velocity

Greek symbols

α	thermal diffusivity (m^2/s)
β	thermal expansion coefficient (1/K)
θ	angle measured from the lower symmetry plane
μ	dynamic viscosity (N s/m^2)
ν	kinematic viscosity (m^2/s)
ρ	density (kg/m^3)
ϕ	nanoparticle volume fraction
Ψ	nondimensional stream function
ψ	dimensional stream function (m^2/s)
Ω	nondimensional vorticity
ω	dimensional vorticity (1/s)

Subscripts

avg	average
C	cold
f	fluid
H	hot
nf	nanofluid
p	particle
o	reference value at cold condition

results conducted on natural convection used the Brinkman model for the viscosity. This model is shown to underestimate the effective viscosity of the nanofluid (Nguyen et al., 2007; Polidori et al., 2007). The Brinkman model does not consider the effect of nanofluid temperature or nanoparticles size. Besides, the Brinkman model was derived for larger particles size compared to the size of the nanoparticles. On the other hand, for the thermal conductivity, most of numerical simulations reported in literature used the Maxwell Garnett (MG) model. This model does not consider main mechanisms for heat transfer in nanofluids such as Brownian motion and does not consider nanoparticle size or temperature dependence. Therefore, numerical simulations need more robust models for viscosity and thermal conductivity that take into account temperature dependence and nanoparticle size. Recently, Nguyen et al. (2007) and Angue Minsta et al. (2009) studied the effect nanoparticles concentration, nanoparticles size on nanofluids viscosity under a wide range of temperatures experimentally. They showed that viscosity drops sharply with temperature especially for high concentration of nanoparticles. Moreover, the effect of temperature, nanoparticle size, and nanoparticles volume fraction on thermal conductivity was studied experimentally by Chon et al. (2005) and they showed that nanofluid thermal conductivity is also affected by temperature, volume fraction of nanoparticles, and nanoparticle size. Thus, such physics cannot be neglected and the dependence of nanofluid properties on temperature, volume fraction of nanoparticles, must be taken into account in order to predict the correct role of nanoparticles on heat transfer enhancement.

Therefore, the scope of the current research is to implement more appropriate models for nanofluids properties and study the effect of these models on heat transfer in natural convection. The experimental results reported by Nguyen et al. (2007) will be used to derive a correlation for nanofluids viscosity as a function of temperature and nanoparticles concentration. Also, the Chon et al. model (2005) will be used for the thermal conductivity. The current research will evaluate the role of both viscosity and thermal conductivity, derived from experimental data, on heat transfer in natural convection. Besides, these models will be compared to frequent used models in literature namely the Brinkman model for viscosity and the MG model for thermal conductivity. The enhancement in heat transfer will be evaluated under wide range of temperatures and wide range of volume fraction of nanoparticles.

2. Governing equations and problem formulation

Fig. 1 shows a schematic diagram of differentially heated annulus. The fluid in the annulus is a water-based nanofluid containing Al_2O_3 nanoparticle. The nanofluid is assumed incompressible and the flow is assumed to be laminar. It is assumed that water and

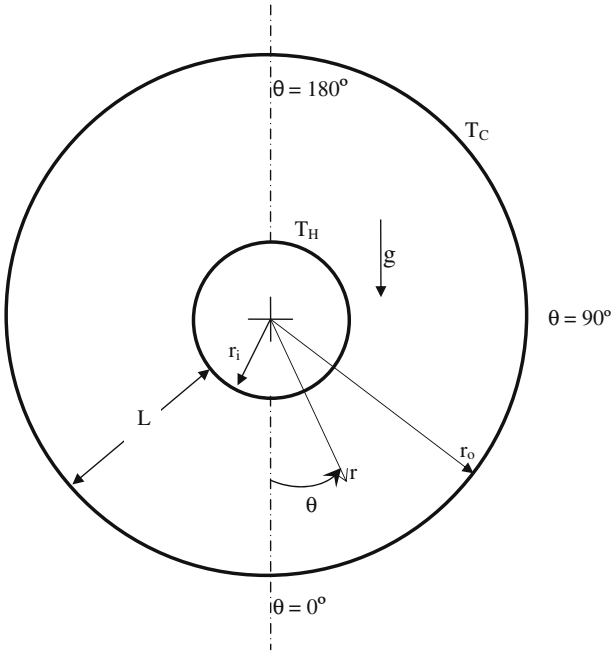

Fig. 1. Sketch of problem geometry.

Table 1
Thermophysical properties of fluid and Al_2O_3 nanoparticles.

Physical properties	Fluid phase (water)	Al_2O_3
c_p (J/kgK)	4179	765
ρ (kg/m^3)	997.1	3970
k (W/mK)	0.613	25
$\beta \times 10^{-5}$ (1/K)	21	0.85
D_p (nm)	0.384	47

nanoparticles are in thermal equilibrium and no slip occurs between them. The thermophysical properties of the nanofluid are given in Table 1. The inner cylinder is maintained at a constant temperature (T_H) higher than the outer cylinder (T_C). The density of the nanofluid is approximated by the Boussinesq model. The viscosity as well as the thermal conductivity of the nanofluid is considered variable properties that vary with temperature and volume fraction of nanoparticles.

The governing equations for the laminar, steady state natural convection in terms of the stream function-vorticity formulation are given as:

Vorticity

$$\frac{\partial}{\partial \tilde{r}}\left(\omega\frac{\partial \Psi}{\partial \theta}\right)-\frac{\partial}{\partial \theta}\left(\omega\frac{\partial \Psi}{\partial \tilde{r}}\right)=\frac{1}{\rho_{nf}}\left(\frac{\partial}{\partial \tilde{r}}\left(\mu_{nf}\tilde{r}\frac{\partial \omega}{\partial \tilde{r}}\right)+\frac{\partial}{\partial \theta}\left(\mu_{nf}\frac{1}{\tilde{r}}\frac{\partial \omega}{\partial \theta}\right)\right)+\frac{(\varphi\rho_s\beta_s+(1-\varphi)\rho_f\beta_f)}{\rho_{nf}}\times g\left(\frac{\partial \tilde{T}}{\partial \tilde{r}}\tilde{r}\sin\theta+\frac{\partial \tilde{T}}{\partial \theta}\cos\theta\right)=0 \quad (1)$$

Energy

$$\frac{\partial}{\partial \tilde{r}}\left(\tilde{T}\frac{\partial \Psi}{\partial \theta}\right)-\frac{\partial}{\partial \theta}\left(\tilde{T}\frac{\partial \Psi}{\partial \tilde{r}}\right)=\frac{\partial}{\partial \tilde{r}}\left(\alpha_{nf}\tilde{r}\frac{\partial \tilde{T}}{\partial \tilde{r}}\right)+\frac{\partial}{\partial \theta}\left(\alpha_{nf}\frac{1}{\tilde{r}}\frac{\partial \tilde{T}}{\partial \theta}\right) \quad (2)$$

Kinematics

$$\frac{\partial}{\partial \tilde{r}}\left(\tilde{r}\frac{\partial \Psi}{\partial \tilde{r}}\right)+\frac{\partial}{\partial \theta}\left(\frac{1}{\tilde{r}}\frac{\partial \Psi}{\partial \theta}\right)=-\tilde{r}\omega \quad (3)$$

The radial and tangential velocities are given by the following relations, respectively,

$$v=\frac{1}{\tilde{r}}\frac{\partial \psi}{\partial \theta}, \quad (4)$$

$$u=-\frac{\partial \psi}{\partial \tilde{r}}. \quad (5)$$

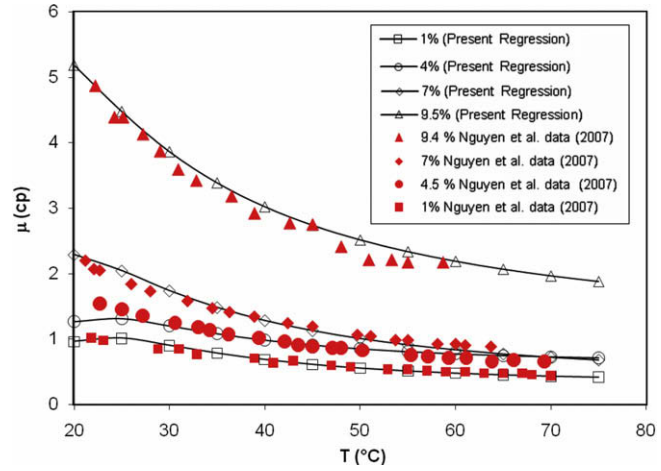

Fig. 2. Comparison between viscosities calculated using Eq. (13) and the Nguyen et al. data (2007).

Table 2
Grid independence tests.

Grid size	Air		Nanofluid	
	Nu_{avg}	Relative error*	Nu_{avg}	Relative error*
21 × 21	2.3925802	–	6.925662	–
31 × 31	2.4544397	0.025203	6.808558	−0.0172
41 × 41	2.4698942	0.006257	6.769043	−0.00584
51 × 51	2.4701051	8.54×10^{-05}	6.772485	0.000508
61 × 61	2.4701027	-9.7×10^{-07}	6.772491	8.86×10^{-07}
71 × 71	2.4701036	3.64×10^{-07}	6.772487	-5.9×10^{-07}
81 × 81	2.4701031	-2×10^{-07}	6.772492	7.38×10^{-07}
101 × 101	2.4701028	-1.2×10^{-07}	6.772489	-4.4×10^{-07}

* Relative error = $(Nu_{\text{large grid}} - Nu_{\text{small grid}})/Nu_{\text{large grid}}$.

The thermal diffusivity, in Eq. (2), is given as:

$$\alpha_{nf}=\frac{k_{nf}}{(\rho c_p)_{nf}} \quad (6)$$

The effective density of the nanofluid is given as

$$\rho_{nf}=(1-\varphi)\rho_f+\varphi\rho_p \quad (7)$$

The heat capacitance of the nanofluid is expressed as:

$$(\rho c_p)_{nf}=(1-\varphi)(\rho c_p)_f+\varphi(\rho c_p)_p \quad (8)$$

The effective thermal conductivity of the nanofluid is calculated by the Chon et al. model (2005):

$$\frac{k_{nf}}{k_{bf}}=1+64.7\varphi^{0.7640}\left(\frac{d_f}{d_p}\right)^{0.3690}\left(\frac{k_f}{k_p}\right)^{0.7476}\mathrm{Pr}^{0.9955}\,\mathrm{Re}^{1.2321} \quad (9)$$

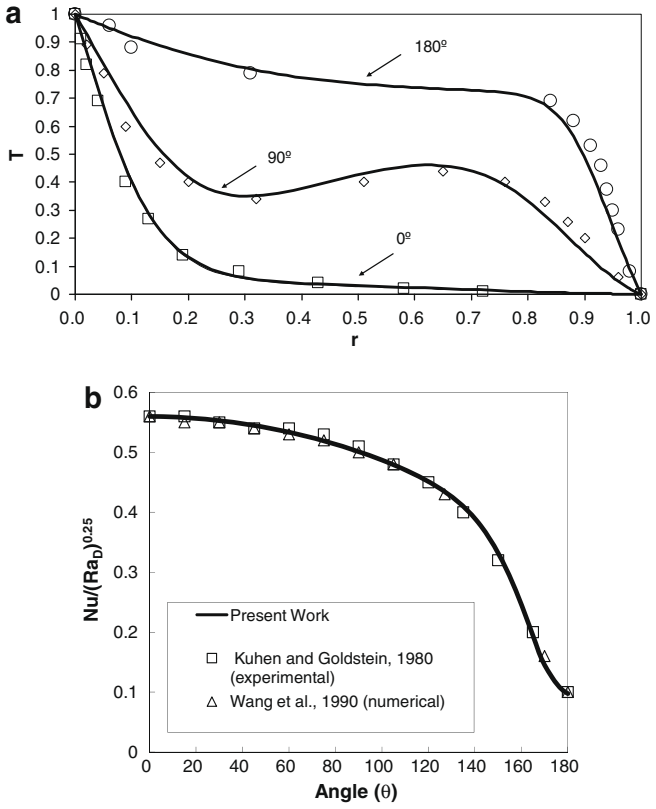

Fig. 3. (a) Comparison of present work (solid lines) and Kuhen and Goldstein experimental results (1976), experimental data points: □: 0°, ◇: 90°, ○: 180° (Ra = 4.7×10^4, Pr = 0.706, and L/D = 0.8). (b) Comparison between present work and other published data for the distribution of Nusselt number around the cylinder surface for pure natural convection case ($Ra_D = 10^5$, Pr = 0.7).

The results using Eq. (9) will be compared to the MG model given by:

$$\frac{k_{nf}}{k_f} = \frac{k_p + (n-1)k_f - (n-1)(k_f - k_p)\varphi}{k_p + (n-1)k_f + (k_f - k_p)\varphi} \tag{10}$$

The Pr and Re in Eq. (9) are given as, respectively (Chon et al., 2005):

$$\mathrm{Pr} = \frac{\mu_f}{\rho_f \alpha_f} \tag{11}$$

$$Re = \frac{\rho_f k_b T}{3\pi\mu_f^2 l_f} \tag{12}$$

where f stands for the base fluid which is water in the current study and k_b is the Boltzmann constant, 1.3807×10^{-23} J/K and l_f is the mean path of base fluid particles given as 0.17 nm (Chon et al., 2005). This model considers the effect of nanoparticle size and temperature on nanofluids thermal conductivity with a wide range of temperature between 21 and 70 °C. This model was further tested experimentally by Angue Minsta et al. (2009) for Al_2O_3 and CuO nanoparticles and found to predict the thermal conductivity of nanofluid accurately up to a volume fraction of 9% for both CuO and Al_2O_3 nanoparticles. Therefore, the current study adopted the Chon et al. model to predict the thermal conductivity of Al_2O_3–water nanofluid.

The correlation for dynamic viscosity of Al_2O_3–water nanofluid is derived using the available experimental data of Nguyen et al. (2007). Actually, no explicit correlation is given in Nguyen et al. (2007) that give the viscosity of Al_2O_3–water nanofluid as a function of the temperature and the volume fraction of nanoparticles simultaneously. Therefore, in the recent work, a two-dimensional regression is further performed on the raw experimental data reported in Nguyen et al. (2007) to develop such a correlation. This derived correlation gives the viscosity of nanofluid as a function of temperature and volume fraction of nanoparticles. The R^2 of the regression is 99.8% and a maximum error is 5%. The correlation, obtained from the two-dimensional regression, is given as:

$$\mu_{Al_2O_3} = -0.155 - \frac{19.582}{\tilde{T}} + 0.794\varphi + \frac{2094.47}{\tilde{T}^2} - .192\varphi^2 - 8.11\frac{\varphi}{\tilde{T}} - \frac{27463.863}{\tilde{T}^3} + .0127\varphi^3 + 1.6044\frac{\varphi^2}{\tilde{T}} + 2.1754\frac{\varphi}{\tilde{T}^2} \tag{13}$$

The viscosity in Eq. (13) is expressed in centi poise. Fig. 2 presents a plot for the viscosity of Al_2O_3–water nanofluid as a function of temperature and concentration of nanoparticles calculated by using Eq. (13). Also, the figure plots the measured data from Nguyen et al. experiment (2007). It is very clear that the current regression is in good agreement with the measurements of Nguyen et al. (2007).

The results, using Eq. (13), will be compared to the Brinkman model given by:

$$\mu_{nf} = \frac{\mu_f}{(1-\varphi)^{2.5}} \tag{14}$$

The following dimensionless groups are introduced:

$$\Omega = \frac{\omega L^2}{\alpha_{f_o}}, \quad \Psi = \frac{\psi}{\alpha_{f_o}}, \quad V = \frac{vL}{\alpha_{f_o}}$$
$$U = \frac{uL}{\alpha_{f_o}}, \quad T = \frac{\tilde{T} - T_C}{T_H - T_C}, \quad \text{and} \quad r = \frac{\tilde{r} - r_i}{L}$$
$$k = \frac{k_{nf}}{k_{fo}}, \quad \alpha = \frac{\alpha_{nf}}{\alpha_{fo}}, \quad \mu = \frac{\mu_{nf}}{\mu_{f_o}} \tag{15}$$

where the subscript "o" stands for the reference temperature which is taken as 22 °C in the current study. The temperature difference between the hot and the cold surfaces is kept constant at 30 °C.

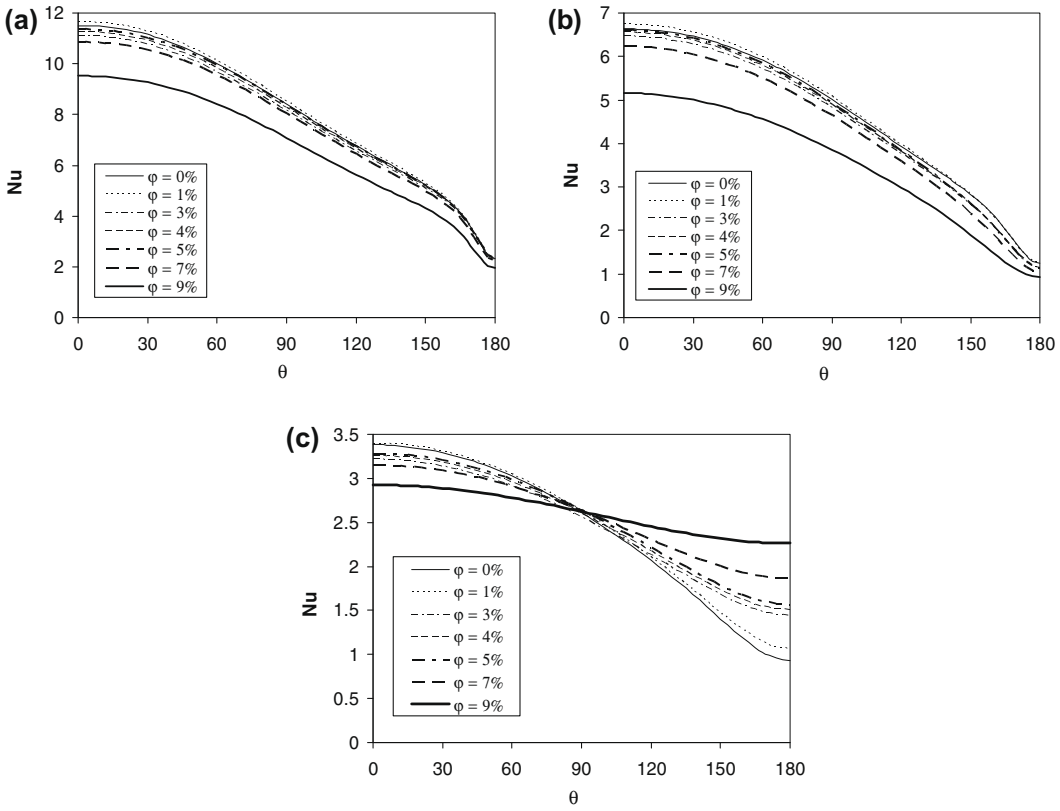

Fig. 4. Nusselt number distribution around inner cylinder surface using various volume fractions of Al_2O_3 nanoparticles, $L/D = 0.8$: (a) Ra = 10^5, (b) Ra = 10^4, and (c) Ra = 10^3.

By using the dimensionless parameters, the governing equations are written as:

$$\frac{\partial}{\partial r}\left(\Omega\frac{\partial \Psi}{\partial \theta}\right)-\frac{\partial}{\partial \theta}\left(\Omega\frac{\partial \Psi}{\partial r}\right) = \frac{\Pr}{(1-\varphi)+\varphi\frac{\rho_p}{\rho_f}}\left(\frac{\partial}{\partial r}\left(\mu\left(r+\frac{r_i}{L}\right)\frac{\partial \Omega}{\partial r}\right)+\frac{\partial}{\partial \theta}\left(\mu\frac{1}{\left(r+\frac{r_i}{L}\right)}\frac{\partial \Omega}{\partial \theta}\right)\right) + \mathrm{Ra}\Pr\left[\frac{1}{\frac{(1-\varphi)}{\varphi}\frac{\rho_f}{\rho_p}+1}\frac{\beta_s}{\beta_f}+\frac{1}{\frac{\varphi}{(1-\varphi)}\frac{\rho_f}{\rho_p}+1}\right]\left(\frac{\partial T}{\partial r}\left(r+\frac{r_i}{L}\right)\sin\theta+\frac{\partial T}{\partial \theta}\cos\theta\right) \quad (16)$$

$$\frac{\partial}{\partial r}\left(T\frac{\partial \Psi}{\partial \theta}\right)-\frac{\partial}{\partial \theta}\left(T\frac{\partial \Psi}{\partial r}\right) = \frac{1}{(1-\varphi)+\varphi\frac{(\rho c_p)_p}{(\rho c_p)_{f_0}}}\left(\frac{\partial}{\partial r}\left(k\left(r+\frac{r_i}{L}\right)\frac{\partial \Omega}{\partial r}\right)+\frac{\partial}{\partial \theta}\left(k\frac{1}{\left(r+\frac{r_i}{L}\right)}\frac{\partial \Omega}{\partial \theta}\right)\right) \quad (17)$$

$$\frac{\partial}{\partial r}\left(r\frac{\partial \psi}{\partial r}\right)+\frac{\partial}{\partial \theta}) = -r\omega \quad (18)$$

where

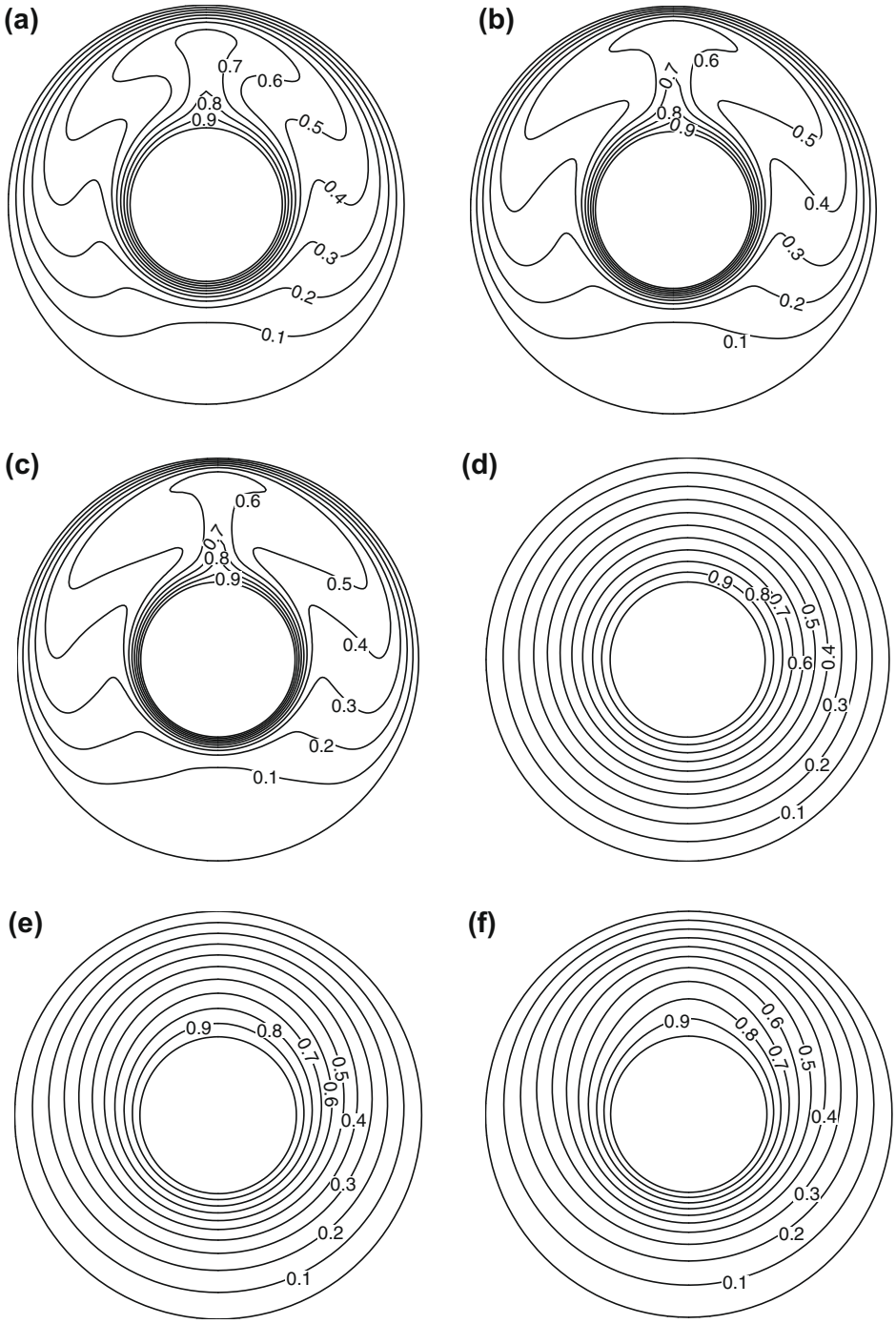

Fig. 5. Temperature isotherms for $L/D = 0.8$: (a) $\mathrm{Ra} = 10^5$ $\phi = 9\%$, (b) $\mathrm{Ra} = 10^5$, $\phi = 4\%$, (c) $\mathrm{Ra} = 10^5$, $\phi = 1\%$, (d) $\mathrm{Ra} = 10^3$, $\phi = 9\%$, (e) $\mathrm{Ra} = 10^3$, $\phi = 4\%$, and (f) $\mathrm{Ra} = 10^3$, $\phi = 1\%$.

$$\mathrm{Ra} = \frac{g\beta(T_H - T_C)L^3}{\nu_{f_o}\alpha_{f_o}} \tag{19}$$

$$\mathrm{Pr} = \frac{\nu_{f_o}}{\alpha_{f_o}} \tag{20}$$

The ratio between the gap length between the inner and outer cylinders divided by the inner cylinder diameter, i.e., L/D, is defined as the aspect ratio. The effective thermal expansion coefficient of the nanofluid appears on the right hand side of Eq. (17) which is given as (Khanafer et al., 2003)

$$\frac{\beta_{nf}}{\beta_f} = \left[\frac{1}{\frac{(1-\varphi)}{\varphi}\frac{\rho_f}{\rho_p}+1}\frac{\beta_p}{\beta_f} + \frac{1}{\frac{\varphi}{(1-\varphi)}\frac{\rho_f}{\rho_p}+1}\right] \tag{21}$$

The dimensionless radial and tangential velocities are given as, respectively:

$$V = \frac{1}{\left(r+\frac{r_i}{L}\right)}\frac{\partial\psi}{\partial\theta}, \qquad U = -\frac{\partial\psi}{\partial r}. \tag{22}$$

Due to the symmetry, only half of the cylinder will be solved (i.e., $0 \leqslant \theta \leqslant 180$). Therefore, the dimensionless boundary conditions are as follows:

On the inner cylinder surface, $\Psi = 0$

$$\omega = -\frac{\partial^2\Psi}{\partial r^2}, \quad \text{and} \quad T = 1$$

On the outer cylinder surface, $\Psi = 0$ (23)

$$\omega = -\frac{\partial^2\Psi}{\partial r^2}, \quad \text{and} \quad T = 0$$

$$\text{Symmetry lines}: \quad \Psi = 0, \quad \Omega = 0, \quad \text{and} \quad \frac{\partial T}{\partial\theta} = 0$$

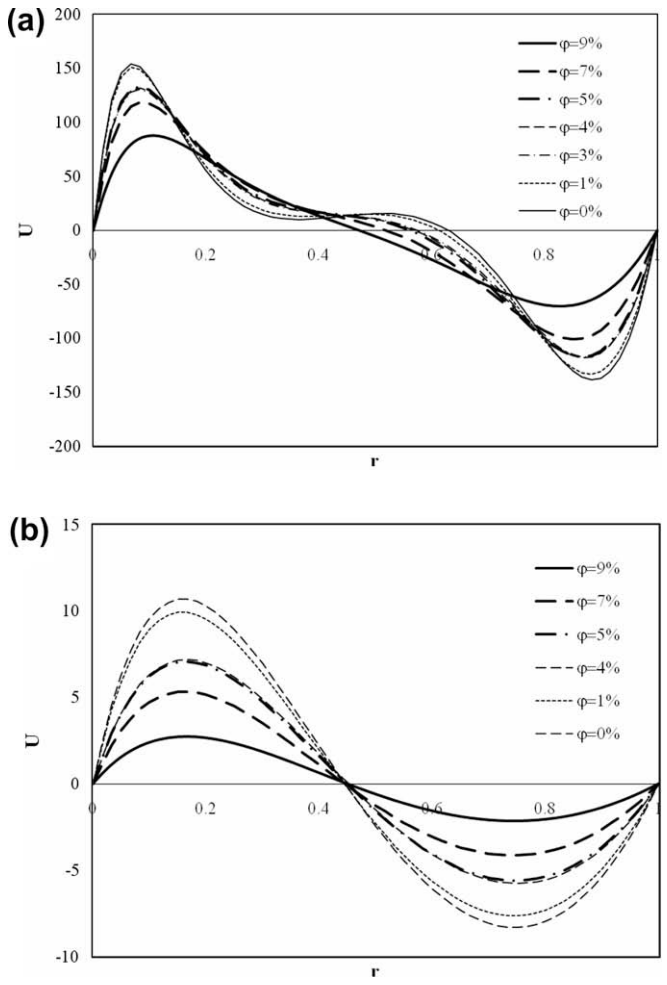

Fig. 6. Tangential velocity for $\mathrm{Ra} = 10^5$, $L/D = 0.8$ $\theta = 90°$: (a) $\mathrm{Ra} = 10^5$ and (b) $\mathrm{Ra} = 10^3$.

3. Numerical implementation

Eqs. (17)–(19) and the variable properties, given by Eqs. (9) and (13), with the boundary conditions given in Eq. (24) are solved using the finite volume approach (Patankar, 1980; Versteeg and Malalasekera, 1995). The diffusion term in the vorticity and energy equations is approximated by a second-order central difference scheme which gives a stable solution and a second-order upwind differencing scheme is adopted for the convective terms. For full details of numerical implementation, the reader is referred to Abu-Nada et al. (2008).

After solving Ψ, Ω, and T, further useful quantities are obtained. For example, the Nusselt number can be expressed as:

$$\mathrm{Nu} = \frac{h(D)}{k_f} \tag{24}$$

The heat transfer coefficient is expressed as

$$h = \frac{q_w}{T_H - T_C} \tag{25}$$

The thermal conductivity is expressed as

$$k_{nf} = -\frac{q_w}{\partial\tilde{T}/\partial\tilde{r}} \tag{26}$$

By substituting Eqs. (26), (27), (9) into Eq. (25), and using the dimensionless quantities, the Nusselt number on the inner cylinder is written as:

$$\mathrm{Nu} = -\left(\frac{k_{nf}}{k_f}\right)\frac{\partial T}{\partial r} \tag{27}$$

where (k_{nf}/k_f) is calculated using Eq. 9. The average Nusselt number is calculated as:

$$\mathrm{Nu}_{avg} = \frac{1}{\pi}\int_{\theta=0}^{\theta=\pi}\mathrm{Nu}(\theta)d\theta \tag{28}$$

The integration of Eq. (27) is carried out by using the 1/3rd Simpson's rule of integration. A normalized Nusselt number is defined as the ratio of Nusselt number at any volume fraction of nanoparticles to that of pure water and is given as:

$$\mathrm{Nu}^*_{avg}(\varphi) = \frac{Nu(\varphi)}{Nu(\varphi = 0)} \tag{29}$$

The Nusselt number is used as an indicator of heat transfer enhancement where an increase in Nusselt number corresponds to enhancement in heat transfer.

4. Grid testing and code validation

An extensive mesh testing procedure was conducted to guarantee a grid independent solution. Two cases of $\mathrm{Ra} = 0.53 \times 10^4$ and $\mathrm{Ra} = 10^5$ using $\mathrm{Pr} = 0.7$ are tested for grid independence with no nanoparticles in the flow field. The present code was tested for grid independence by calculating the average Nusselt number around the inner cylinder surface. It was found that a grid size of 61×61 guarantees a grid independent solution for both cases.

The Nusselt number for the grid independent solution is compared with the results of Guj and Stella (1995) and Shu et al. (2000) for concentric horizontal annulus and Ra = 0.53×10^4. The calculated average Nusselt number by the current code gives a value of 2.47010 which falls between the results obtained by Guj and Stella (Nu_{avg} = 2.4220) and the results of Shu et al. (Nu_{avg} = 2.5560). Furthermore, a grid independence test was carried out for the Al_2O_3–water nanofluid using ϕ = 9%, Ra = 10^5, and L/D = 0.8. It was found that the same grid size 61×61 guarantees a grid independent solution. Details of grid independence solution are given in Table 2.

Due the lack of experimental data for natural convection in an annulus with the presence of nanoparticles, the present numerical solution is validated by the experimental results of Kuhen and Goldstein (1976) using Ra = 4.57×10^4 and Pr = 0.7. The comparisons for three temperature profiles at three different angles are shown in Fig. 3a. Furthermore, another validation test was carried for pure natural convection of air around a heated horizontal cylinder in free air for Ra = 10^5 and Pr = 0.70 with the experiment of Kuhen and Goldstein (1980) and the numerical work of Wang et al. (1990) as shown in Fig. 3b. It is clear that present results are in good agreement with other published data.

5. Results and discussion

The range of Rayleigh number, volume fraction of nanoparticles, and expansion ratio, are Ra = 10^3–10^5, $0 \leqslant \phi \leqslant 9\%$, and $0.2 \leqslant L/D \leqslant 0.8$, respectively. Fig. 4 presents Nusselt number distribution around the inner cylinder surface using various volume fractions of Al_2O_3 nanoparticles for L/D = 0.8. For the case of Ra = 10^5 and Ra = 10^4 the increase in the volume fraction of nanoparticles causes a reduction in Nusselt number every where around the inner cylinder surface. However, for Ra = 10^3 there is a reduction in Nusselt number for $\theta < 90$ and an enhancement in heat transfer is taking place for $\theta > 90$. The difference between ϕ = 1% and the pure fluid case is negligible whereas the effect of nanoparticles become more evident at higher concentrations. Also, it is clear that for high volume fraction of nanoparticles, ϕ = 9%, and for the case for Ra = 10^3, the Nusselt number variation around the inner cylinder surface becomes less pronounced compared to lower volume fraction of nanoparticles. Actually, for Ra = 10^3, the more addition of nanoparticles reduces the difference between the maximum and minimum Nusselt number around the cylinder surface. For example, for ϕ = 9% the maximum Nusselt number is 2.9 and the minimum is 2.3. This is best illustrated by looking at Fig. 5 where the case of ϕ = 9%, and for the case for Ra = 10^3 the temperature is almost uniform around the inner cylinder surface. Also, Fig. 5 illustrates how the thickness of thermal boundary layer is influenced by the addition of nanoparticles. Also, it is very interesting to note how the plume region is affected by increasing the volume fraction for nanoparticles where for the case of 10^5, as shown in Fig. 5a, the plume region spreads wider and for the case of Ra = 10^3, as shown in Fig. 5d, the plume region disappears completely. This behavior is related to the increased viscosity at high volume fraction of nanoparticles, see Fig. 2, where high ϕ causes the fluid to become more viscous and this causes the velocity to decrease accordingly, see Fig. 6, which reduces convection. Fig. 6 shows how the maximum

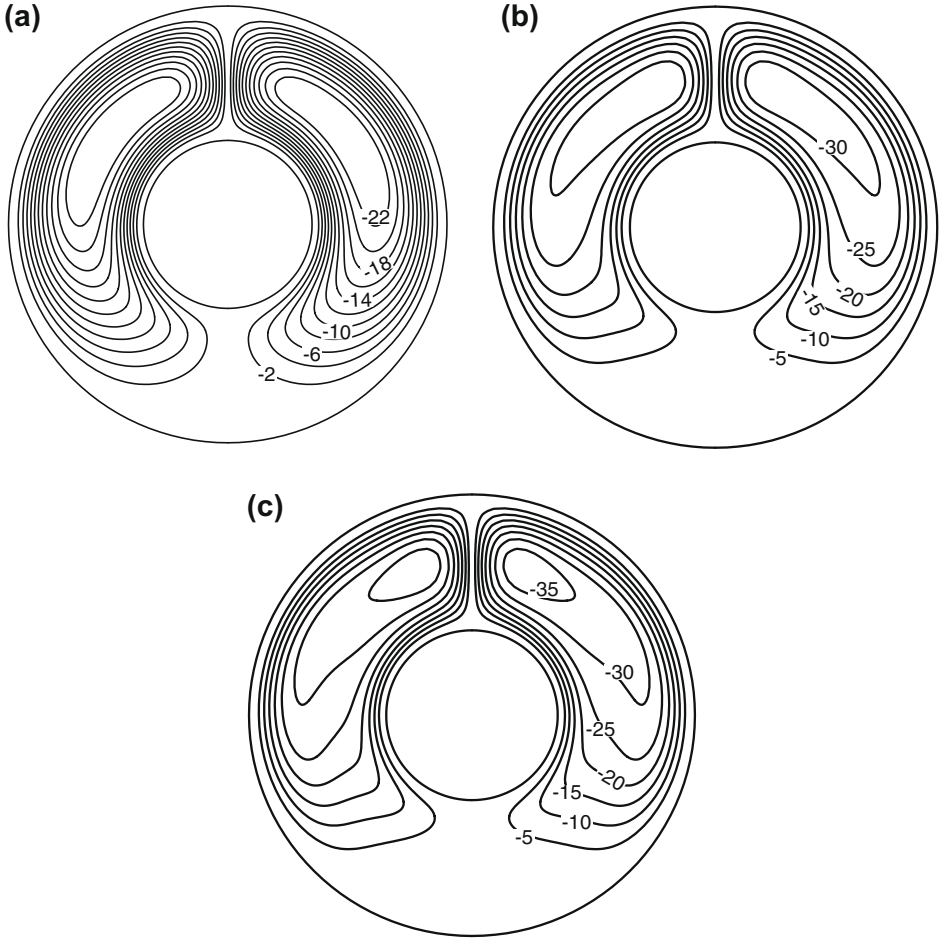

Fig. 7. Streamlines for Ra = 10^5, L/D = 0.8: (a) ϕ = 9%, (b) ϕ = 4%, and (c) ϕ = 1%.

velocity drops to almost one half when the volume fraction of nanopartilces is increased from zero (clear fluid) to 9% for the case of Ra = 10^5. Also, Fig. 6 shows that this reduction becomes more severe at Ra = 10^3 where the maximum velocity drops to almost one fourth of the maximum velocity when the volume fraction of nanopartilces is increases from zero to 9%. Besides, Fig. 6 reveals how the velocity gradients at the inner cylinder wall are affected by presence of nanopartilces. This velocity gradient change will affect the convection around the inner cylinder surface and accordingly will influence the Nusselt number around the inner cylinder. The reduction in velocities and convection will cause the fading of the plume at Ra = 10^3 and the spreading of the plume region for the case of Ra = 10^5. The increase of thermal boundary layer thickness is responsible for the reduction in temperature gradients at the inner surface which causes a reduction in Nusselt number accordingly, see Eq. (29). It is observed from Fig. 5, for Ra = 10^5, that the addition of nanoparticles causes an increase in thermal boundary layer thickness which explains the reduction in the value of Nusselt number every where around the inner cylinder surface. However, for the case of Ra = 10^3, the addition of nanoparticles causes the thermal boundary layer thickness to increase for $\theta < 90$; however, this thickness decreases for $\theta > 90$ because of the plume disappearance. This explains the behavior observed in Fig. 4c for the Nusselt number distribution around the inner surface. Fig. 7 shows the streamlines for the case of Ra = 10^5. It is clear that by increasing the volume fraction of nanoparticles the maximum strength of streamlines is reduced due to the increased viscosity of the nanofluids as mentioned earlier.

Fig. 8 studies the effect of addition of nanoparticles on Nusselt number by using different aspect ratios for the annulus. The figure shows that for the case of Ra = 10^5, the behavior encountered using smaller aspect ratio is similar to that of high aspect ratio. However, for Ra = 10^3 different behavior is observed using smaller aspect ratios. For the case of Ra = 10^3 the angle at which Nusselt number switches from a reduction to increasing is reduced to 60° for $L/D = 0.4$ and to an almost complete enhancement all over the

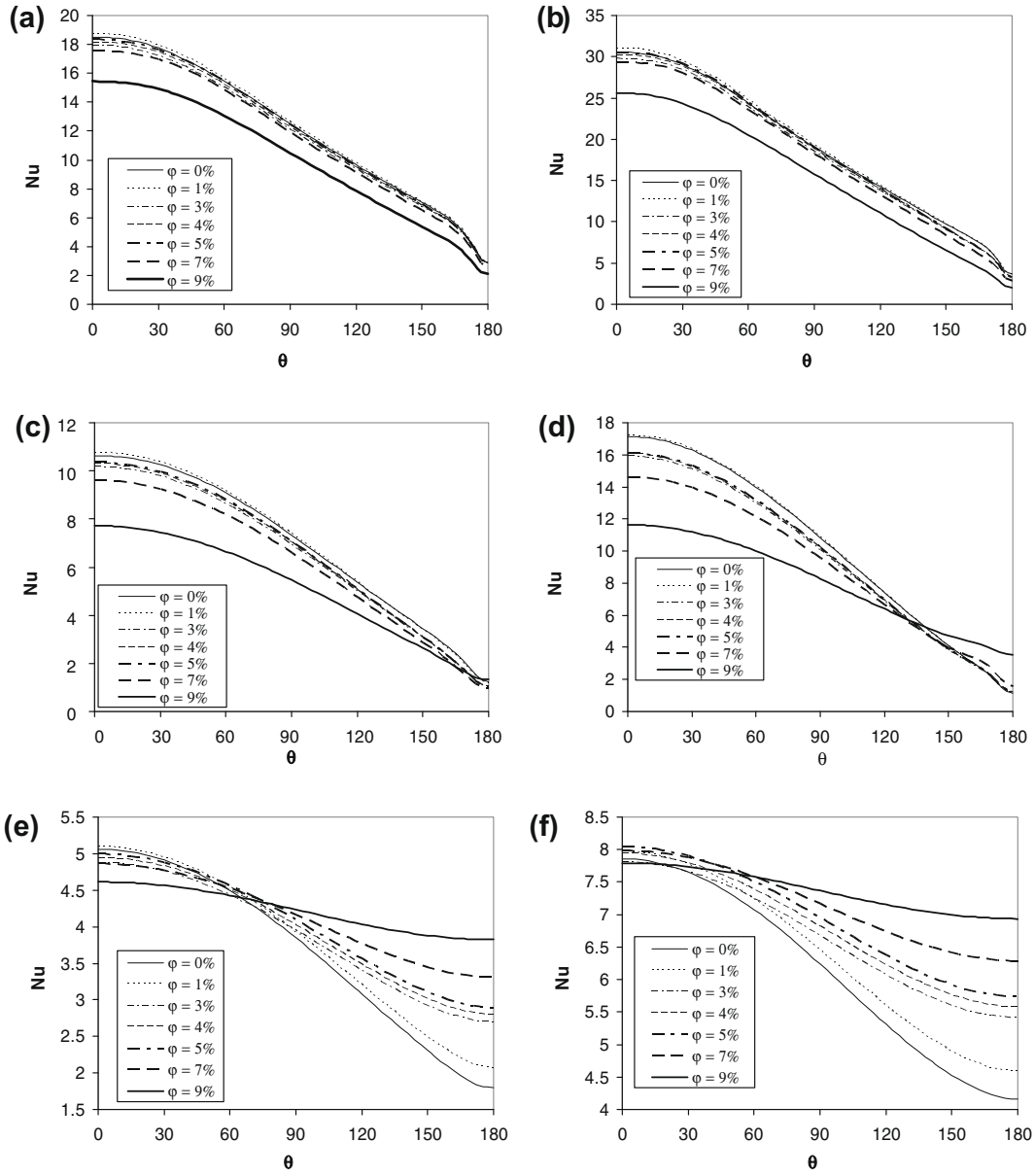

Fig. 8. Nusselt number distribution around inner cylinder surface using various volume fractions of Al_2O_3 nanoparticles: (a) Ra = 10^5, $L/D = 0.4$, (b) Ra = 10^5, $L/D = 0.2$, (c) Ra = 10^4, $L/D = 0.4$, (d) Ra = 10^4, $L/D = 0.2$, (e) Ra = 10^3, $L/D = 0.4$, and (f) Ra = 10^3, $L/D = 0.2$.

cylinder surface for $L/D = 0.2$ compared to the 90° encountered at $L/D = 0.8$; see Fig. 4. Thus, the region around the inner cylinder surface where an enhancement in heat transfer is taking place increases. This causes an enhancement in the total Nusselt number around the inner cylinder surface as shown in Fig. 9.

Fig. 9 shows the average Nusselt number as well as normalized average Nusselt number around the inner cylinder surface. It is observed that, for all expansion ratios, and for the case of $Ra = 10^4$ and $Ra = 10^5$ a decrease in Nusselt number is taking place for volume fraction of nanoparticles greater than 5%. However, such a decrease is not observed for volume fraction less than 5% where a fluctuation in Nusselt number is detected. In general, the influence of nanoparticles has two opposing effects on Nusselt number: a favorable effect that is due to the presence of high thermal conductivity of nanoparticles and an undesirable effect due to the high level of viscosity experienced at high volume fraction of nanoparticles. The heat transfer in natural convection at high Rayleigh number is dominated by convection and at low Rayleigh numbers is dominated by conduction. So, for $Ra = 10^5$ and 10^4, the heat transfer is dominated by convection and the presence of nanoparticles will cause the nanofluid to become more viscous which will reduce convection currents and accordingly temperature gradient at the cylinder surface and Nusselt number. This will be accompanied by some enhancement in heat transfer due to the high thermal conductivity of nanoparticles. However, such enhancement is small compared to the deterioration caused by viscosity because the convection currents in the annulus will be reduced, see Fig. 7. In fact, the role of Brownian motion becomes less pronounced because the thermal conductivity of nanofluid is inversely proportional to the viscosity squared as shown in Eq. (12). Therefore, for high Rayleigh number the more addition of nanoparticles, for $\phi > 5$, will have an adverse effect on Nusselt

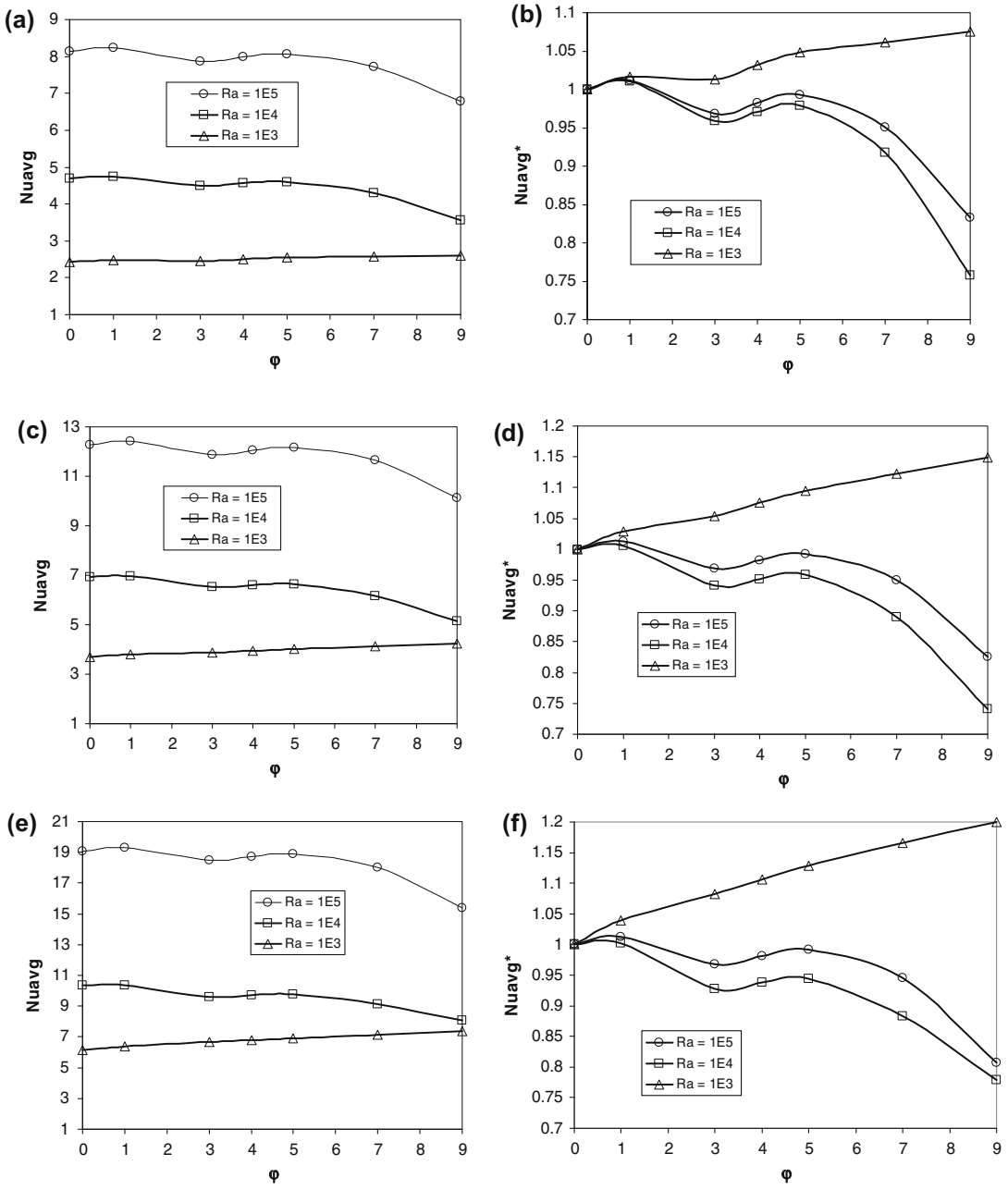

Fig. 9. (a) Average Nusselt number $L/D = 0.8$, (b) normalized Nusselt number $L/D = 0.8$, (c) average Nusselt number $L/D = 0.4$, (d) normalized Nusselt number $L/D = 0.4$, (e) average Nusselt number $L/D = 0.2$, (f) normalized Nusselt number $L/D = 0.2$.

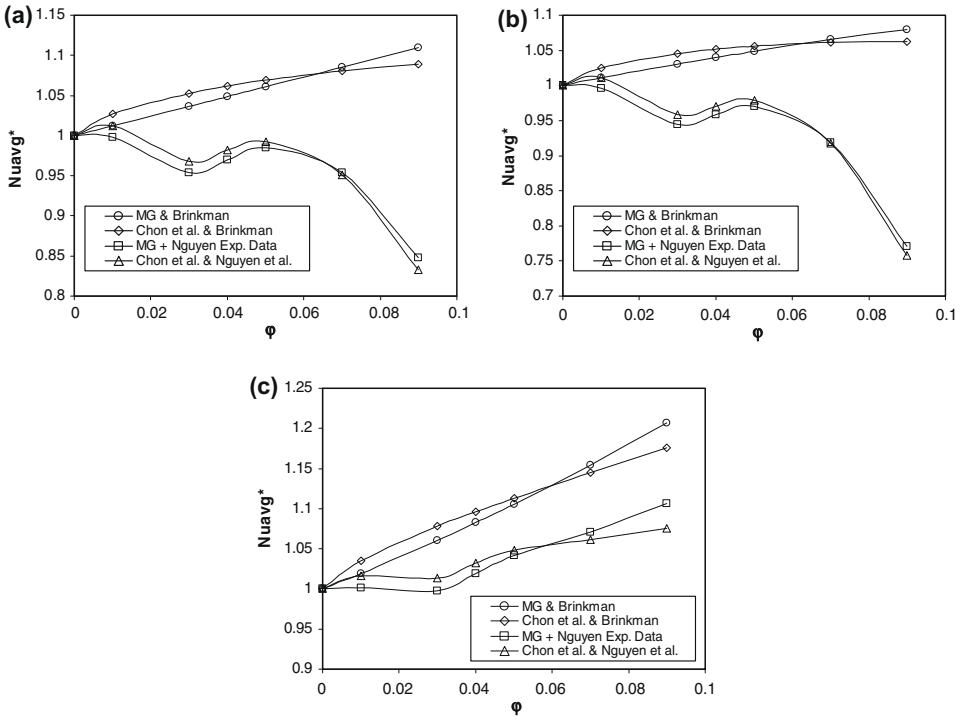

Fig. 10. Effect of the conductivity and viscosity models on Nusselt number, $L/D = 0.8$: (a) Ra = 10^5, (b) Ra = 10^4, and (c) Ra = 10^3.

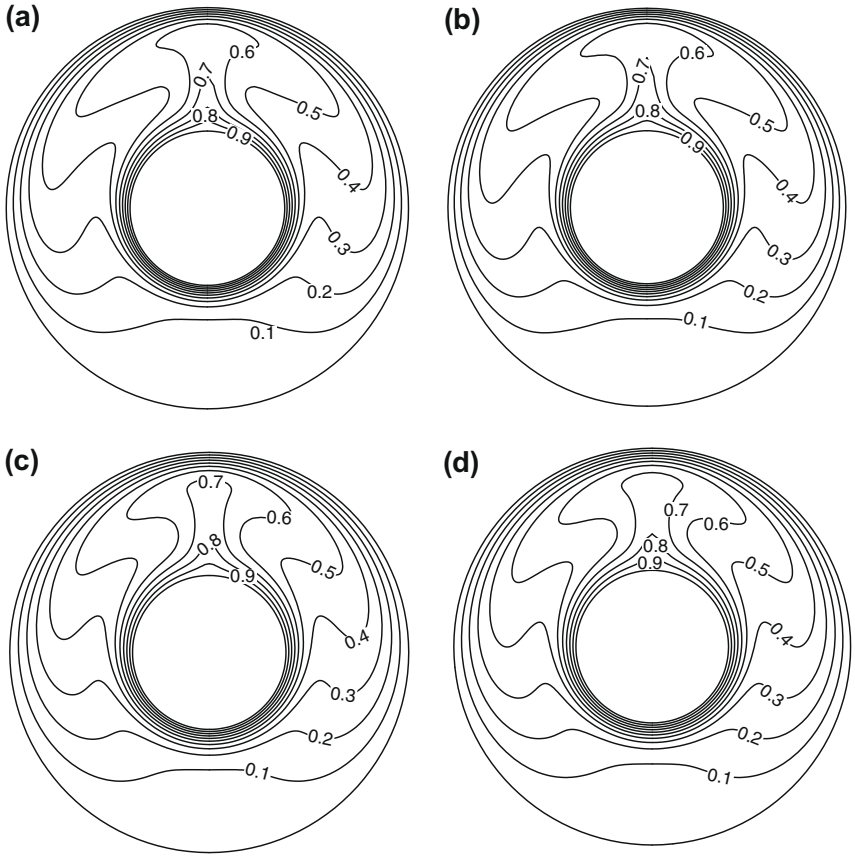

Fig. 11. Isotherms for Ra = 10^5, $L/D = 0.8$, $\phi = 9\%$: (a) MG and Brinkman model, (b) Chon et al. model (2005) and Brinkman model, (c) MG model and Nguyen et al. data (2007), and (d) Chon et al. model (2005) and Nguyen et al. data (2007).

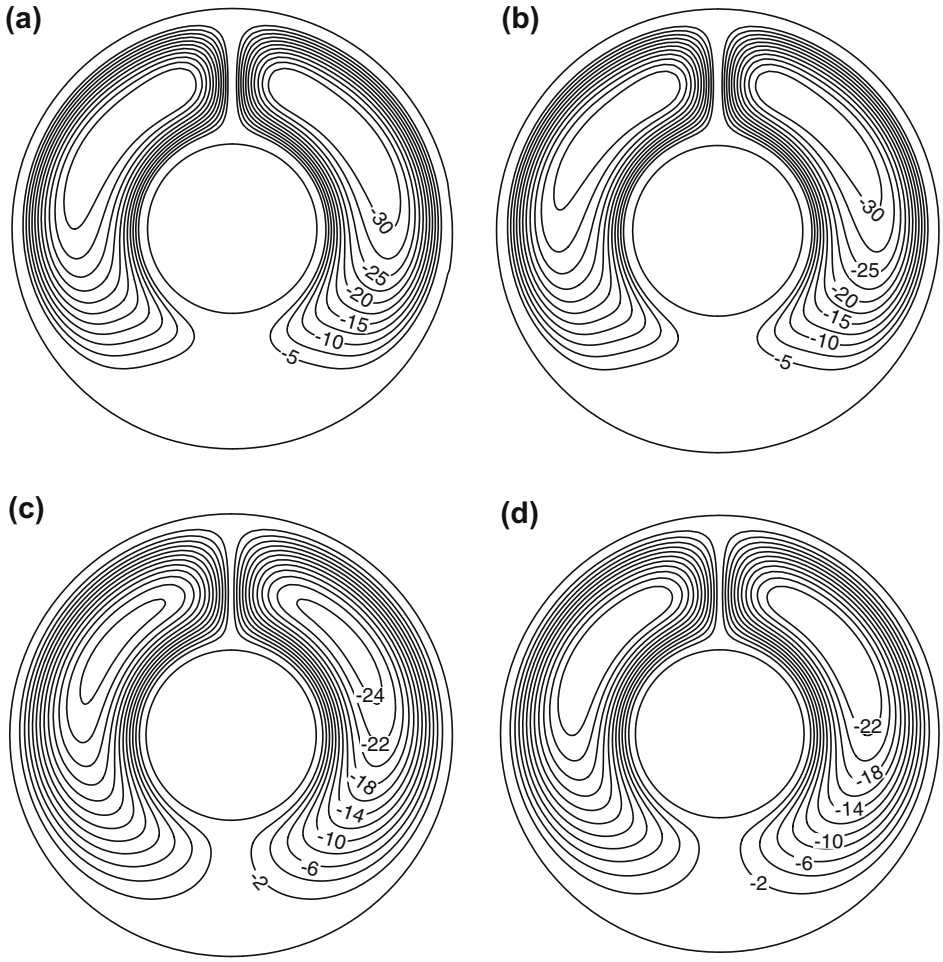

Fig. 12. Streamlines for Ra = 10^5, $L/D = 0.8$, $\phi = 9\%$: (a) MG and Brinkman model, (b) Chon et al. model (2005) and Brinkman model, (c) MG model and Nguyen et al. data (2007), and (d) Chon et al. model (2005) and Nguyen et al. data (2005).

number. However, for $\phi \leqslant 5$, the role of viscosity is less pronounced and the adverse effect of viscosity is sort of balanced by the favorable effect of thermal conductivity which explains the fluctuation in Nusselt number for $\phi \leqslant 5$. Also, it is worth to mention that the case of Ra = 10^4 experience more deterioration in Nusselt number compared Ra = 10^5. Actually, for Ra = 10^4 the inertia forces are smaller than that of Ra = 10^5 which will cause the adverse effect of nanoparticles to become more severe at Ra = 10^4 which will cause more reduction in Nusselt number compared to Ra = 10^5.

On the other hand, for low Rayleigh numbers i.e., Ra = 10^3, the heat transfer is dominated by conduction and by adding more nanoparticles the conduction is enhanced due to the high thermal conductivity of nanoparticles and accordingly the heat transfer is enhanced. The more addition of nanoprtilces will cause the strong convection currents that are mainly experienced in the plume regions to diminish which will cause a disappearance of the plume region, see Fig. 5d–f. This will cause an increase in temperature gradient all over the cylinder surface and accordingly an increase in Nusselt number.

An interesting comparison between various models used for thermal conductivity and viscosity on the average Nusselt number is shown in Fig. 10. This figure shows results obtained using four different approaches. The first approach is using MG model for the thermal conductivity and Brinkman model for the viscosity of nanofluids. This combination is used by most researchers in literature. The second approach is using the Chon et al. model (2005) for thermal conductivity and the Brinkman model for the viscosity of the nanofluid. The third approach is using the MG model for the thermal conductivity and the experimental data of Nguyen et al. (2007) for viscosity. The fourth approach, the one that is used in the current study as the base case, is using the Chon et al. model (2005) for thermal conductivity and Nguyen et al. model for viscosity of nanofluids. From Fig. 10a and b, it is clear that difference between average Nusselt number calculated using the Chon et al. model and the MG model is relatively small. However, the difference in Nusselt number when using the Nguyen et al. data and Brinkman model is much more significant. This tells that the effect of thermal conductivity models is less significant than viscosity models at high Rayleigh number. So, the prediction of Nusselt number using the Nguyen data is completely different from using the Brinkman model. According to the Brinkman model prediction, there is an over estimation in the enhancement in Nusselt number by increasing the volume fraction of nanoparticles. However, the Nguyen et al. data shows deterioration in Nusselt number by adding nanoparticles. Actually, the Brinkman model is used for dispersed particles in solution with particle size much higher than the nano-scale particles and its applicability to nanoparticles is questionable. On the other hand for low Rayleigh number, i.e., Ra = 10^3 when Nguen et al. data is used the Nusselt number is not sensitive to volume fraction less than 4%; however, for higher volume fractions an enhancement in heat transfer is observed which is opposite to the behavior registered at high Rayleigh number (using the Nguyen et al. data). It is interesting to note that for this Rayleigh number all of the four approaches predict an enhancement in heat transfer. Also, the difference in Nusselt pre-

diction between the Brinkman model and the Nguyen et al. data is small compared to high Rayleigh numbers. For example, the maximum difference, at $\phi = 9\%$, is approximately 10% compared to 30% at $Ra = 10^5$.

Also, Fig. 10 shows that the deviation between the Chon et al. model and MG model becomes more pronounced for $Ra = 10^3$ especially at high volume fractions of nanoparticles. This tells that such difference becomes more appreciable at high volume fraction of nanoparticles and this difference cannot be neglected. In general the MG model over predicts the enhancement in heat transfer compared to the Chon et al. model at high volume fractions of nanoparticles ($\phi > 5\%$). Fig. 10 is very useful to know when the MG model is appropriate for natural convections applications and when its applicability becomes less accurate. Besides, it tells that for higher Rayleigh numbers the Brinkman prediction is far from Nguyen et al. measured data prediction and this difference cannot be neglected which limits the applicability of Brinkman model for these Rayleigh numbers. However, this difference is less pronounced at lower Rayleigh number and the Brinkman model could be used with approximately 10% deviation in prediction from the measured data. Figs. 11 and 12 show the isotherms and the streamlines for the four mentioned approaches, respectively. It is very clear how different models give different temperature and streamlines distribution in the annulus.

6. Conclusions

For $Ra \geqslant 10^4$ and $\phi > 5\%$, the average Nusselt number is reduced by increasing the volume fraction of nanoparticles. However, the influence of nanoparticles is less pronounced at low volume fraction where a fluctuation in Nusselt number is noticed for $\phi \leqslant 5\%$. For $Ra = 10^3$, the average Nusselt number is enhanced by increasing the volume fraction of nanoparticles. Generally speaking, for $Ra \geqslant 10^4$, the Nusselt number is deteriorated every where around the cylinder surface especially at high expansion ratio. However, this reduction is only limited to certain regions around the cylinder surface at $Ra = 10^3$. For $Ra \geqslant 10^4$, the difference in MG and Chon et al. model prediction is small. However, there is a deviation at $Ra = 10^3$ and this deviation becomes more significant at high volume fraction of nanoparticles. The Nguyen data and Brinkman model gives completely different predictions for $Ra \geqslant 10^4$ where the difference in prediction of Nusselt number could more than 30%. However, this difference reduces to less than 10% at $Ra = 10^3$.

References

Abu-Nada, E., Masoud, Z., Hijazi, A., 2008. Natural convection heat transfer enhancement in horizontal concentric annuli using nanofluids. Int. Commun. Heat Mass Transfer 35 (5), 657–665.

Angue Minsta, H., Roy, G., Nguyen, C.T., Doucet, D., 2009. New temperature and conductivity data for water-based nanofluids. Int. J. Therm. Sci. 48 (2), 363–371.

Choi, U.S., 1995. Enhancing thermal conductivity of fluids with nanoparticles. In: Siginer, D.A., Wang, H.P. (Eds.), Developments and applications of non-Newtonian flows, FED-vol. 231, pp. 66, 99–105.

Chon, C.H., Kihm, K.D., Lee, S.P., Choi, S.U.S., 2005. Empirical correlation finding the role of temperature and particle size for nanofluid (Al2O3) thermal conductivity enhancement. Appl. Phys. Lett. 87 (97), 153107.

Daungthongsuk, W., Wongwises, S., 2007. A critical review of convective heat transfer nanofluids. Renewable Sustainable Energy Rev. 11, 797–817.

Guj, G., Stella, F., 1995. Natural convection in horizontal eccentric annuli: numerical study. Numer. Heat Transfer A 27, 89–105.

Khanafer, K., Vafai, K., Lightstone, M., 2003. Buoyancy-driven heat transfer enhancement in a two-dimensional enclosure utilizing nanofluids. Int. J. Heat Mass Transfer 46, 3639–3653.

Kuhen, T.H., Goldstein, R.J., 1976. An experimental and theoretical study of natural convection in the annulus between horizontal concentric cylinders. J. Fluid Mech. 74, 695–719.

Kuhen, T.H., Goldstein, R.J., 1980. Numerical solutions to the Navier–Stokes equations for laminar natural convection. Int. J. Heat Mass Transfer 23, 971–979.

Mansour, R. Ben, Galanis, N., Nguyen, C.T., 2007. Effect of uncertainties in physical properties on forced convection heat transfer with nanofluids. Appl. Therm. Eng. 27 (1), 240–249.

Nguyen, C.T., Desgranges, F., Roy, G., Galanis, N., Mare, T., Boucher, S., Angue Minsta, H., 2007. Temperature and particle-size dependent viscosity data for water-based nanofluids – hystresis phenomenon. Int. J. Heat Fluid Flow 28, 1492–1506.

Oztop, H.F., Abu-Nada, E., 2008. Numerical study of natural convection in partially heated rectangular enclosure filled with nanofluids. Int. J. Heat Fluid Flow 29 (5), 1326–1336.

Patankar, S.V., 1980. Numerical Heat Transfer and Fluid Flow. Hemisphere Publishing Corporation, Taylor and Francis Group, New York.

Polidori, G., Fohanno, S., Nguyen, C.T., 2007. A note on heat transfer modeling of Newtonian nanofluids in laminar free convection. Int. J. Therm. Sci. 46 (8), 739–744.

Putra, N., Roetzel, W., Das, S.K., 2003. Natural convection of nano-fluids. Heat Mass Transfer 39, 775–784.

Shu, C., Yeo, K.S., Yao, Q., 2000. An efficient approach to simulate natural convection in arbitrary eccentric annuli by vorticity stream function formulation. Numer. Heat Transfer A 38, 739–756.

Trisaksri, V., Wongwises, S., 2007. Critical review of heat transfer characteristics of nanofluids. Renewable Sustainable Energy Rev. 11, 512–523.

Versteeg, H.K., Malalasekera, W., 1995. An Introduction to Computational Fluid Dynamic: The Finite Volume Method. John Wiley & Sons Inc., New York.

Wang, P., Kahawita, R., Nguyen, T.H., 1990. Numerical computation of the natural convection flow about a horizontal cylinder using splines. Numer. Heat Transfer A 17, 191–215.

Wen, D., Ding, Y., 2006. Natural convective heat transfer of suspensions of titanium dioxide nanoparticles (nanofluids). IEEE Trans. Nanotechnol. 5 (3), 220–227.